Published in final edited form as:
NMR Biomed. 2011 February ; 24(2): 114–129. doi:10.1002/nbm.1570.

Fluorine (^{19}F) MRS and MRI in biomedicine

Jesús Ruiz-Cabello[a,b,c], **Brad P. Barnett**[a,b], **Paul A. Bottomley**[a], and **Jeff W.M. Bulte**[a,b,d,e,*]

[a] Russell H. Morgan Department of Radiology, Division of MR Research, Johns Hopkins University School of Medicine, Baltimore, MD, USA

[b] Vascular Biology Program and Cellular Imaging Section, Institute for Cell Engineering, Johns Hopkins University School of Medicine, Baltimore, USA

[c] NMR Group, Institute of Functional Studies, Complutense University and CIBERES, Madrid, Spain

[d] Department of Biomedical Engineering, Johns Hopkins University School of Medicine, Baltimore, MD, USA

[e] Department of Chemical and Biomolecular Engineering, Johns Hopkins University School of Medicine, Baltimore, MD, USA

Abstract

Shortly after the introduction of ^{1}H MRI, fluorinated molecules were tested as MR-detectable tracers or contrast agents. Many fluorinated compounds, which are nontoxic and chemically inert, are now being used in a broad range of biomedical applications, including anesthetics, chemotherapeutic agents, and molecules with high oxygen solubility for respiration and blood substitution. These compounds can be monitored by fluorine (^{19}F) MRI and/or MRS, providing a noninvasive means to interrogate associated functions in biological systems. As a result of the lack of endogenous fluorine in living organisms, ^{19}F MRI of 'hotspots' of targeted fluorinated contrast agents has recently opened up new research avenues in molecular and cellular imaging. This includes the specific targeting and imaging of cellular surface epitopes, as well as MRI cell tracking of endogenous macrophages, injected immune cells and stem cell transplants.

Keywords

perfluorocarbon; MR contrast agent; lung ventilation; oxygen measurement; molecular imaging; cellular imaging

INTRODUCTION

The ^{19}F nucleus has a 100% natural abundance and resonates at a resonant frequency that is 94% of that of ^{1}H. Its NMR sensitivity is 83% of that of ^{1}H (with constant noise), so that its MRI signal-to-noise ratio (SNR) is about 89% of ^{1}H per nucleus, assuming sample-dominant noise (i.e. the noise increases linearly with frequency). There is negligible endogenous ^{19}F MRI signal from the body, as the physiological concentrations of detectable mobile fluorine are below the detection limit (usually less than 10^{-3} μmol/g wet tissue weight). Fluorine exists at higher concentrations in the bone matrix and teeth, but, being

*Correspondence to: J. W. Bulte, Russell H. Morgan Department of Radiology and Radiological Science, Johns Hopkins University School of Medicine, 217 Traylor Bldg, 720 Rutland Ave., Baltimore, MD 21205-2195, USA. jwmbulte@mri.jhu.edu.

immobilized, exhibits a very short spin–spin relaxation time (T_2) that is not visible to conventional MRI methods. This lack of background signal provides ^{19}F MRI with a potentially extremely high contrast-to-noise ratio and specificity, if a fluorinated compound can be introduced as a contrast agent.

However, for ^{19}F MRI to produce an image quality similar to that of ^{1}H MRI, whose signal derives from nearly two-thirds of all nuclei present in the body, the agent requires a very high density of ^{19}F nuclei on the molecule in addition to a high tissue concentration. To achieve the former, perfluorination offers the attraction of providing a comparable density of ^{19}F nuclei when all ^{1}H nuclei on a hydrocarbon chain are replaced.

Perfluorocarbons (PFCs) are molecules of similar structure to common organic compounds (e.g. alkanes), except that all of the hydrogen atoms are replaced by fluorine. These agents have a number of interesting properties that are well suited for medical applications. In addition, fluorine is the most electronegative element in the Periodic Table, and therefore the synthetic introduction of fluorine into contrast agents can produce dramatic electronic perturbations and modify sterical tertial structures.

HISTORICAL PERSPECTIVE

Some of the current potential applications of ^{19}F imaging and spectroscopy for obtaining functional information in living systems were suggested in the 1970s (1), around the time of the first human ^{1}H MRI applications. The first ^{19}F images of NaF, and a PFC, perfluorotributylamine (PFTA), in phantoms are shown in Fig. 1. ^{19}F MRI of biocompatible fluorinated compounds thus represents one of the earliest examples of MRI contrast agents (2). Around the same time, fluorinated drugs appeared on the market and the properties of PFCs were being investigated. Several PFCs were developed during World War II as part of the Manhattan Project to isolate the isomers of uranium. One of their most important biological properties, their high oxygen affinity, was recognized in the 1960s, when mice and cats were shown to survive complete immersion in oxygenated PFCs, followed by long-term survival without apparent ill-effects (3). However, it was not until the 1980s that the chemical inertness of PFCs and, more specifically, their inability to be metabolized were fully documented. One problem with regard to the biological use of many PFC species is that they are insoluble in water. This is routinely addressed for a variety of medical applications by preparing PFCs as water emulsions (4).

The ^{19}F MRI properties of many fluorinated compounds in pharmaceutical, anesthesiological and oncological applications have been discussed in other excellent reviews and book chapters (5–13). In this review, special emphasis is placed on emerging applications, including the use of PFCs for molecular imaging and cell tracking, as well as for studying lung function.

GENERAL PROPERTIES OF PFCs

As noted above, liquid PFCs have a low water solubility [e.g. perfluoro-octyl bromide (PFOB) has a maximal water solubility of 10^{-9} M], which leads to slow diffusion and a long tenancy at the target site of the compound in its natural form. Although PFCs are lipophobic, because the degree of lipophobicity is commonly less than the hydrophobicity, PFCs tend to partition into the lipid component of cellular membranes and, in some cases, affect the cellular response to certain stimulants and stressors. The depth of penetration and the penetration rate can be modulated as a function of the particle size and the lipid solubility of emulsions prepared with different PFCs. PFCs are also characterized by a very low surface tension, which make them attractive for certain applications (e.g. intra-alveolar). An effective fluidity (viscosity) and a positive coefficient of spreading allow these molecules to

spread evenly over a surface. For example, they could spread homogeneously into the entire lung, and potentially form a barrier around target cells to seal and prevent further growth of a malignant disorder. The water–PFC interfacial tension is around 60 mN/m (14), which explains the difficulty in preparing stable emulsions. The stability of the emulsion is directly proportional to the water solubility. PFCs also have a high density and compressibility, which provide a natural cushion between opposing surfaces to reduce the contact force, as well as high volatility and low polarizability. The combination of these properties with their low water solubility makes them ideally suited for use as injectable emulsions of PFC-containing gas, for example, in contrast agents for ultrasound imaging, or for the intravenous delivery of hyperpolarized gases in perfusion and functional MRI studies (15).

The main applications for PFCs as exogenous contrast agents for ^{19}F NMR can be divided into two categories. First, PFCs can be detected and quantified directly by ^{19}F NMR. Second, PFCs can be used for the indirect observation of molecular level changes in biologically important molecules or environmental factors as a result of their influence on fluorine nuclei. The first group of applications, based on the direct detection of fluorinated molecules, includes functional lung imaging (using gases such as SF_6, C_2F_6, CF_4, C_3F_8 and liquid PFCs), cell tracking using PFC emulsions and *in vivo* monitoring of fluorinated drugs and their metabolites. An example is the use of ^{19}F MRS techniques for the detection of 5-fluorouracil (5-FU), a chemotherapeutic agent (16). As a result of the low tissue concentration of 5-FU (in the μmol/g wet weight range) and fluorine-containing pharmaceuticals used at clinical doses, the sensitivity of ^{19}F MRS and MRI depends primarily on the number of fluorine atoms present in the compound and the dose, in addition to the conventional factors that determine SNR, such as the magnetic field strength, detector design, etc.

The second group of applications includes examples in which the fluorine molecules respond to a specific parameter, such as the presence of ligands. Fluorinated compounds are capable of detecting changes in oxygen, H^+ (pH), Na^+, Ca^{2+} and Mg^{2+}concentrations in biological tissues, and may therefore provide proxy measurements of these (17). Of particular interest are the paramagnetic relaxation effects imparted by oxygen on ^{19}F nuclei, which cause changes in the spin–lattice relaxation rates ($1/T_1$), and can alter the chemical shift of one or more of the fluorine moieties. Changes associated with temperature and blood flow in the microenvironment may also affect the ^{19}F signals. In addition to the limits imposed by the low *in vivo* ^{19}F concentration of the agent being used, the utility of the ^{19}F agent as a proxy largely depends on the magnitude and sensitivity of the changes that are elicited.

Also included in this second group is the use of fluorinated emulsions in ^{1}H MRI applications. One type of PFC, PFOB, has been shown to be an effective negative contrast agent for delineating the bowel and improving bowel wall visualization (18,19). The bowel lumina appear homogeneously black on T_1-and T_2-weighted MR images because of the insolubility of PFOB in water and intestinal secretions. Paramagnetic nanoparticles that combine gadolinium diethylenetriaminepentaacetate (Gd-DTPA) and PFC have also been developed for molecular imaging of fibrin (20), and as a platform for delivering a very large number of Gd^{3+} ions to targeted binding sites (21).

PREPARATION AND CHEMICAL STABILITY OF PFCs

The PFCs used in biomedical applications are chemically inert. They are derived synthetically, consist primarily of carbon and fluorine atoms, and are typically clear, colorless liquids that are insoluble in water. They must therefore be emulsified for clinically relevant applications involving intravenous injection, intraperitoneal injection, tissue

intraparenchymal injection or administration in oxygen-permeable biodegradable and biocompatible capsules. The process is analogous to the routine preparation of lipid emulsions for parenteral nutrition. Despite the intrinsically low solubility, diffusivity, density and interfacial surface tension of PFCs, it is possible to generate stable nanoparticles of these compounds using a high-pressure micro-emulsifier. The latter deagglomerates and disperses submicrometer PFC particles uniformly in the fluid. This results in a smaller particle size compared with unpressurized emulsification, which, in turn, permits higher PFC concentrations – 40% and higher – to be achieved. The nanoparticles obtained with this procedure typically have a very small size (~ 200 nm). However, the stability of commercially available PFC preparations varies greatly, and there is a direct relationship between PFC stability and the clearance time from the body.

From a design standpoint, most clinical applications require stable preparations that are rapidly cleared from the body. For this reason, PFCs are commonly combined in commercial products to optimize the stability and clearance profile. For example, perfluorodecalin (PFDC) is rapidly cleared from the body, but forms emulsions that have poor stability. However, perfluorotripropylamine (PFTPA) forms stable emulsions that have a long retention time. By combining these two agents, emulsions such as Fluosol® achieve both a clinically acceptable stability and clearance profile. Nevertheless, Fluosol® remains stable for only 6 h after PFDC and PFTPA are mixed. Consequently, PFDC and PFTPA emulsions are stored frozen in separate solutions, and the solutions are thawed and mixed immediately prior to use. For practicality and other reasons, this version of the product was replaced in 1994 by a new PFDC/PFTPA preparation, Oxygent®, that has proved to be much more stable, and does not require frozen storage.

As noted above, the most useful and versatile formulations are a compromise between body clearance, emulsion stability and, for MRI/MRS applications, the maximum number of chemically equivalent fluorine atoms. Perfluoropolyethers (PFPEs) (e.g. containing 12, 15 or 18 crown ethers) are excellent ^{19}F MRI contrast agents as they provide a single sharp resonance, eliminating any chemical shift artifact, maximizing the SNR and allowing an unambiguous identification of the PFC. Nanoparticle preparations of some of these agents are thermodynamically stable (they do not coalesce) and can be prepared using several different types of emulsifying agent that form a film around the dispersed globules of PFC. Typical emulsifying agents are surface-active agents, adsorbing at oil–water interfaces to form monomolecular films that reduce the interfacial surface tension. A large variety of agents have been used to improve the stability (lecithin is one of the most commonly used) and to increase the effective encapsulation of PFCs. In practice, combinations of emulsifiers are commonly used, rather than a single agent (e.g. safflower oil and lecithin, cholesterol and lecithin, etc.) (22,23). This enables the modification and optimization of the balance between the hydrophilic and lipophilic parts of the emulsifier or mixture of emulsifiers.

The addition of other agents to a PFC emulsion can improve its performance from an MRI/MRS standpoint, but can also affect the stability of the preparation. For example, adding a paramagnetic element that reduces the ^{19}F NMR T_1 values improves the signal intensity and SNR efficiency, by enabling the acquisition of a larger number of scans with a shorter pulse sequence repetition period (TR) in the same scan time. Adding fluorescent lipids, cationic transfection reagents (lipofectamine) or targeted ligands to PFCs provides a means to detect the agents by fluorescence microscopy, to enhance cellular labeling or to perform molecular imaging, respectively (21,23,24). A number of drugs, including antibacterial agents, vasoactive bronchodilators, mucolytic agents, glucocorticoids, antineoplastic agents and DNA, have also been incorporated into PFC emulsions without reducing their stability (25). These drugs offer a lot of ‘bang for the buck’ as the PFC phase can contain a high payload of hydrophobic drugs.

GAS SOLUBILITY OF PFCs

As mentioned earlier, emulsions of these molecules can dissolve significant quantities of relatively small molecules that have a low cohesivity, i.e. gases. Emulsified PFCs can transport and deliver oxygen, CO_2, N_2, NO, etc., with a solubility in the PFC that is independent of temperature. Unlike hemoglobin, which binds O_2 through a covalent bond to its iron atoms, oxygen is not bound but dissolved by the PFC carrier. The oxygen-carrying capacity of an emulsified PFC, such as PFDC/PFTPA, is around three times that of blood at 25°C, and the CO_2-carrying capacity is approximately four times greater than that for oxygen.

The dissolved oxygen has paramagnetic properties that affect the relaxation rate, $R_1 = 1/T_1$, of fluorine nuclei in linear proportion to the dissolved oxygen concentration, although the temperature and magnetic field also play a role (17). This allows the MRI monitoring of partial pressure of O_2 (pO_2) effects, including the possibility of using ^{19}F as a proxy for determining the tissue oxygenation state, or even for generating a proxy image of the oxygen distribution in an organ. When perfluorinated compounds are used as contrast media in these applications, their distribution reflects the region of blood flow and tissue perfusion, providing selective imaging of influx or efflux analogous to that of a radiographic tracer. The selective imaging of blood flow and perfusion has potential applications for the identification of ischemic and/or nonperfused necrotic tissue. The high solubility of other inert gases, such as xenon (^{129}Xe), in PFC emulsions enables its use as a vehicle for the intravenous delivery of hyperpolarized gas for high-SNR, high-resolution imaging of the perfused tissue (15).

The high gas solubility in PFC emulsions has been used for other applications, such as an *in vivo* nitrous oxide (NO) sink (26). Certain PFC formulations have been Food and Drug Administration (FDA)-approved for human use in media that support microbubbles that reflect sound waves and serve as contrast agents for ultrasound imaging. These are currently in use for the diagnosis of cardiac wall motion abnormalities. The dissolved gas bubbles are small enough to pass through the capillary beds, and are not destroyed when injected into the circulation, as usually happens with nonemulsified air bubbles.

^{19}F MRS OF PFCs

Most NMR applications in MRI and MRS use the ^1H signal from endogenous tissue water and mobile hydrocarbons, but other nuclei have also been employed for MRI. ^{19}F MRI enjoys the advantages of the nucleus' high gyromagnetic ratio (γ = 40.05 MHz/T), spin 1/2, 100% natural isotopic abundance and the fact that it is not a particularly rare (or expensive) element. The similarity of ^{19}F's γ to that of ^1H is another advantage, to the extent that measurements can often be performed with the same MRI scanner as used for conventional ^1H MRI, with the same receiver electronics but retuned radiofrequency coils. Fluorine also has a similar van de Waals' radius to hydrogen (1.2 *vs* 1.35 A $^{\circ}$). When a single hydrogen atom is replaced with fluorine, the change typically does not cause significant conformational changes, although fluorination usually increases the lipophilicity and thus enhances the bioavailability of new drugs. However, as noted above, the substitution of a large number of fluorine atoms in a specifically designed molecule influences the structure and function of this new molecule. Fortunately, for NMR, PFCs have magnetic susceptibilities comparable with that of water.

For ^{19}F MRS, the most challenging aspect is quantification, for both technical and biological reasons (the concentrations of some drugs are prone to underestimation because some, such as fluoxetine, are highly bound to plasma proteins, and thus have very short T_2 values and are 'MRS-invisible'). Most of the *in vivo* MRS data have been generated with surface coils,

which have associated with them the problems of a rapid loss in SNR with distance from the surface coil, and nonuniform excitation fields, both of which hamper quantification. Some common methods that facilitate quantification are the use of adiabatic excitation pulses, coil sensitivity mapping techniques and the use of concentration references. Traditional decoupling and nuclear Overhauser enhancements have been applied for quantitative carbon (^{13}C) and phosphorus (^{31}P) MRS and can also be used to improve ^{19}F SNR (27), although the differences between the gyromagnetic ratios of ^{1}H and ^{19}F are small. All MRS methods are sensitive to local magnetic field variations because of tissue magnetic susceptibility. Magnetization transfer methods may also be applied to investigate the fraction of fluorinated compounds that are bound. The detection limits depend on the particular application. For *in vivo* studies, applications requiring high spatial localization of ^{19}F signals from low-concentration fluoro compounds may not be feasible in practical or tolerable scan times.

^{19}F MRS OF DRUG METABOLISM

^{19}F MRS provides a highly specific tool for the investigation of drugs and their metabolic byproducts that contain fluorine atoms, which is also potentially suitable for quantification. The most commonly used drugs in ^{19}F NMR are listed in Table 1. Their relative ^{19}F SNRs, when present at a tissue concentration of 1 μmol/g wet weight, are also listed.

The study of such drugs by ^{19}F MRI/MRS tends to focus on their chemical structure, anabolism, catabolism, distribution and pharmacokinetics *in vivo* and in excised tissues. As an example, ^{19}F MRS has been used widely in pharmacokinetic studies of the anticancer drug 5-FU. 5-FU was proposed as a prototypical antineoplastic agent (28), with the first MRS work using this drug conducted in the late 1970s (29) and early 1980s (30). Since then, numerous studies in both animal models and in humans, and in different tissues and biological fluids, including plasma and urine, have been presented (31). These studies have facilitated an understanding of the metabolic aspects and cytotoxic activity of this drug.

As an anticancer agent, 5-FU has been applied in concomitant radiotherapy and chemotherapy of different neoplastic diseases, particularly for neoplasms of the colorectal system, the head and neck, the trunk and some breast cancers (11,12,31–37). As a result of the intrinsic toxicity of 5-FU, different pro-drugs (a drug in its nonactive form) of the molecule have been designed to pass intact through the gastrointestinal tract, ultimately localizing and selectively converting to 5-FU in the malignant tissue, based on the higher activity of thymidine phosphorylase (38). Capecitabine is one such protodrug designed in an oral formulation to provide higher accumulation of 5-FU in the tumor, whilst reducing the exposure of healthy tissues to 5-FU.

^{19}F MRS OF EXTRACELLULAR pH AND CATIONS IN CELLS AND TISSUES

^{19}F MRS is also useful for observing biological processes in complex systems, such as the maintenance of intracellular pH in different cell lines (39), and intracellular free calcium and magnesium levels via fluorinated chelates. A good exogenous pH indicator must have favorable pharmacokinetics, i.e. an ionizable group with a p*K* value in the physiological range, good sensitivity and specificity, low toxicity, efficient cell penetration, fast exchange between acid and base forms, but slow exchange across cell membranes, and a large chemical shift range (10,40–43). The intracellular uptake and concentration must be high enough to provide adequate SNR from just the intracellular space. A number of pH indicators have now been investigated (42).

The intracellular concentration of different cations can also be obtained from the change in the ^{19}F NMR spectrum of an indicator cation to which it is bound (44). Ca^{2+} plays an important role as a second messenger in living cells. ^{19}F-based methods have been proposed

for the determination of cytosolic calcium in cells and tissues. One of the more exciting approaches for the detection of this cellular cation is the use of 1,2-bis(*o*-amino-phenoxy)ethane-*N*,*N*,*N*′,*N*′-tetraacetic acid (BAPTA) (45). Here, the ^{19}F-NMR Ca^{2+} indicator is derived from its symmetrically 5,5-substituted difluoro-derivative (FBAPTA) (46), which exhibits a chemical shift response on binding calcium. One of the critical issues for intracellular interrogation of any reporter molecule is the loading of the reporter molecule into cells. As tetracarboxylate does not penetrate the cell, a lipophilic agent, such as acetoxymethyl, is used. Other ^{19}F-bearing ligands have been proposed for ions such as Na^+, Mg^{2+}, Zn^{2+}. Pb^{2+}, etc., as recently reviewed in ref. (17).

FUNCTIONAL LUNG 19F MRI USING GASES AND VOLATILE COMPOUNDS

^{19}F MRI of the lungs was reported in the literature in the early 1980s (47). Recent interest may have been rekindled by new applications involving hyperpolarized noble gases. The possibility of imaging ^{19}F gases directly, together with the unique properties of these compounds, has enabled the measurement of several functional parameters, such as airspace size (via the apparent diffusion coefficient), regional oxygen partial pressure, ventilation distribution, ventilation/perfusion ratios and gas exchange, including oxygen uptake (48–52).

Despite the fact that fluorinated gases offer much less SNR when compared with hyperpolarized gases, fluorinated gases are easy to manage, can be mixed with oxygen, do not involve a polarizing apparatus and are low in price, all of which are advantageous in the context of functional lung MRI performed with inert gases. In particular, fluorinated gases at thermal equilibrium polarization, such as sulfur hexafluoride (SF_6), hexafluoroethane (C_2F_6), tetrafluoromethane (CF_4), and fluoropropane (C_3F_8), have recently been presented as alternatives to hyper-polarized gases that can be mixed with 20% oxygen for continuous breathing without requiring a hyperpolarization apparatus, resulting in a considerable advantage in cost and effort (see Table 2).

SF_6 is one of the more widely used fluorinated molecules in the clinical setting, in addition to the anesthetic halothane [CF(3) CHBrCl]. It has been used in clinical trials as part of a multiple inert gas elimination technique, and as a microbubble contrast agent in ultrasound imaging (Sonovue®). It is a heavy molecule (146.06 g/mol) with six chemically equivalent fluorine atoms. Its low solubility in water is similar to that of ^{3}He (49). Although its higher fluorine count per molecule compared with the MRI-active nuclei on other inhaled gases is an advantage, its very short T_2 and T_1 relaxation times of around 2 ms, together with a much lower diffusivity than that of ^{3}He, make ^{19}F MRI applications employing SF_6 gas very challenging, especially with respect to system gradient and bandwidth requirements. Despite the short relaxation times, some dynamic (53) and diffusion-weighted (48,54) images have been successfully recorded from animal studies.

The use of fluoroethane (C_2F_6, Fig. 2) and fluoropropane (C_3F_8) gases, with relatively longer T_1 and T_2 values of 10 and 20 ms, respectively, seems more promising and more suitable than SF_6 for measurements of diffusion in human lungs with ^{19}F MRI (50,55,56). Indeed, fluoropropane (Optison®– an injectable liquid suspension) is currently used for ultrasound imaging of the internal organs and other anatomical structures in humans.

USE OF PFCs AS BLOOD SUBSTITUTES AND AEROSOLS

As noted above, physiologically important gases, such as oxygen and carbon dioxide, are highly soluble in many PFCs, and do not react with them. These physical properties, together with the reduced need for allogeneic blood transfusion and the facilitation of

oxygen transfer from red cells to the tissue, are central to the utility of PFC emulsions as blood substitutes (see Table 3).

High oxygen levels can also limit the use of PFC blood substitutes to the extent that their oxygen transport characteristics differ from those of blood (57,58). The ^{19}F signals of a number of biological PFCs exhibit R_1 values that depend on oxygen content, thereby potentially providing a measure of the percentage oxygenation. Thus, targeted cell-specific PFC-bearing nanoparticles could potentially provide a means of assessing regional oxygen content, to the extent that the PFC is in contact with the oxygen and the nanoparticle itself does not interfere with the interaction.

PFCs, alone or in a mixture with surfactants, have been used for liquid ventilation (59,60) and drug delivery during liquid ventilation (61). These kinds of applications have been investigated for possible therapeutic use in the treatment of various respiratory diseases, and were the subject of a recent symposium on PFC applications (62,63). As mammals use gas rather than liquid ventilation, PFC vaporization has been developed for the respiratory circuit. Aerosolization appears to be an efficient way to facilitate pulmonary gas exchange in acute respiratory distress syndrome (64).

SENSITIVITY AND DETECTION LIMITS FOR ^{19}F MRI OF PFCs

Organofluoro compounds are rare in nature, which makes the interpretation of studies on how exogenous organofluorides behave *in vivo* less complicated. However, the concentrations of PFCs normally introduced into biological systems are low, and thus typical ^{19}F MRI SNR is low when compared with ^{1}H MRI (see Tables 1–3). Although the use of large quantities of highly fluorinated fluoro compounds can yield high-quality ^{19}F images, high doses (more than 1–5 g/kg for PFCs) may be limited in humans by safety concerns. To date, MRS studies in a whole-body scanner suggest a minimum detectable limit of ^{19}F at 1.5 T of about 30 μmol/g wet weight in a volume of about 33 mL in 6 min (65), based on surface coil measurements following the infusion of 5-FU chemotherapy. This concentration is difficult to achieve with systemic agents, or by passive accumulation of *in vivo* agents. Other authors have reported a detection threshold for spectroscopic 5-FU quantification of about 5 nmol/g in 0.5–1.2-g samples at 11.7 T, albeit with a 1-h data acquisition (38). Our own MRI experience with perfluoro-crown ether (PFCE), which contains 20 chemically equivalent ^{19}F nuclei, indicates that the sensitivity of this compound *in vivo* in a 9.4-T magnet is around 30 μmol/g wet weight in a 4-min acquisition time in a volume of 60 μL (66). Partlow *et al*. (67) have made specific measurements of the detection limit of PFC-labeled cells using ^{19}F MRS and MRI at high (11.7 T) and low (1.5 T) fields. The lower detection limit was found to be 2000 cells for PFCE- and 10,000 cells for PFOB-labeled cells for *in vitro* ^{19}F MRS, and around 6000 PFCE-labeled cells for *in vitro* ^{19}F MRI. Quantification of PFCs revealed intracellular concentrations of up to 3 pmol per cell for a 12-h incubation, without the help of any transfection agent.

Given the linear relationship between signal intensity and PFC concentration (as well as voxel size), it is possible to dramatically increase the final PFCE concentration using targeted nanoparticles containing multiple PFCE molecules. The specific binding of such targeted nanoparticles can increase the local concentration above the minimum detection limit, potentially enabling their use as contrast agents on clinical systems with clinically relevant scan times (23).

OPTIMAL ^{19}F MRI PULSE SEQUENCES FOR PFCs

^{19}F MRS and MRI have been demonstrated with compounds that exhibit several peaks in their NMR chemical shift spectra (e.g. PFTA, PFOB). For fluoro compounds, the ^{19}F

chemical shift dispersion (in Hz) is typically larger than that of ^{1}H. When the ^{19}F signal is divided among several peaks, the ^{19}F MRI SNR may be reduced when compared with a monochromatic spectrum. In addition, if the bandwidth per ^{19}F image pixel is less than the chemical shift dispersion, chemical shift artifacts can arise, wherein the signal from each peak is shifted into a different voxel, creating a 'ghost' image, and/or the location of a selected slice may be displaced in space to a different extent for each moiety (Fig. 1). This is the case for PFOB and PFTA, thus complicating the use of these molecules. Chemically selective imaging pulse sequences can be employed to circumvent the chemical shift artifact problem by excluding the signals from the other peaks, but this does not compensate for the SNR loss. In addition, the relatively short T_2 and the further splitting of the resonances of each moiety in some of these molecules as a result of *J*-modulation (68,69) can further reduce SNR through signal decay and/or increased receiver bandwidth requirements, even at short TE.

Another problem for ^{19}F MRI acquisition is the relatively long T_1 relaxation times of many fluorinated molecules (1–4 s), which necessitates lengthy TR intervals for the recovery of appreciable longitudinal magnetization (69,70). This makes time-efficient and clinically relevant ^{19}F MRI challenging. ^{19}F MRI pulse sequences are typically performed using ultrafast imaging methods, such as keyhole techniques or echo planar imaging (EPI). Ultrafast, low-angle, rapid acquisition and relaxation enhancement is utilized where short TEs are needed, including the use of linear PFPE molecules with small T_2/T_1 ratios (71), and is even useful when the T_2 relaxation time is not a problem (as is the case with PFCE or hexafluorobenzene) (69,72). These sequences can easily be combined with an inversion recovery pulse sequence for T_1 measurements to increase their acquisition efficiency. Although some investigators have proposed the use of paramagnetic contrast agents to shorten the ^{19}F T_1 relaxation times of water-miscible ^{19}F molecules (73,74), this approach is problematic because most PFCs are immiscible in water. Thus, when 15% w/w Gd-DTPA is incorporated into a 20% (w/v) PFCE nanoparticle emulsion (as the bisoleate acid Gd-DTPA-BOA), a small (~ 15%) reduction in T_1 is achievable, but is accompanied by a much larger reduction in T_2 (85%), such that the use of long-TE sequences is no longer an option. The implementation of parallel imaging techniques for ^{19}F MRI also offers scope for improving the ^{19}F acquisition efficiency in the coming years.

MOLECULAR AND CELLULAR 19F MRI

MRI is able to visualize cells *in vivo* in real time. When cells are imaged in living animals, it can provide new insights into the biology of cell trafficking and migration. An example is the homing of white blood and hematopoietic cells in cancer and immunological diseases. Because MRI methods are noninvasive, they can be applied repeatedly to monitor targeted cells and cellular processes. For cells to be visualized by MRI, they generally must be labeled to enable their discrimination from surrounding tissue.

For ^{1}H MRI, superparamagnetic iron oxides (SPIOs) offer one method of magnetic labeling that disturbs the local magnetic field near excited spins (75). The proton signals from water close to SPIO particles are seen as regions of hypointensity, acting as signal voids. However, it is sometimes difficult to discriminate between targeted molecules or cells and image artifacts arising from susceptibility and/or other effects associated with the MRI pulse sequences. Superparamagnetic contrast agents that can provide a positive signal also exist with some MRI techniques, such as on- (76) and off- (77,78) resonance saturation. However, similar problems can arise as those occurring with hypointense contrast.

Another alternative that generates positive contrast is the use of paramagnetic contrast agents, typically gadolinium chelates, that shorten the T_1 relaxation times. Paramagnetic

contrast agents suffer from a relatively high threshold for detection. Much effort has been directed towards the development of intracellular labeling methods that allow sufficient uptake without affecting cellular proliferation or function. Fluorine agents and ^{19}F imaging could present opportunities for labeling with minimal effects on cell proliferation, function and maturation, whilst permitting ^{19}F label-based quantification. A recent article provides a comparative evaluation of the use of various fluorine-containing nanoemulsions for MRI cell tracking (79).

One important article demonstrated the first cellular ^{19}F MRI of passively fluorine-labeled macrophages, which appeared as 'hotspots' in the central nervous system in experimental allergic encephalomyelitis (80). This is an animal model for multiple sclerosis which is characterized by infiltration of the macrophages into the inflamed brain. After induction of the disease, cells were observed after intravenous injection of a PFCE emulsion at 3 g/kg. PFCs have also been used to image macrophage infiltration in the infarcted myocardium (see Fig. 3) (81). This work is similar in concept to ^{1}H MRI studies of the uptake of ultra-small SPIO particles by macrophages in inflammatory diseases. 'Hotspot' ^{19}F MRI of cells gained renewed interest after Ahrens and coworkers (22,71,82) presented an approach to 'active' cell labeling and MRI cell tracking of immune cells *in vivo* (Fig. 4).

Recently, this approach has been extended further to the tracking of stem cells (66,67). Using different PFC preparations with different ^{19}F spectral frequencies (as 'signatures'), it was suggested that multiple cell populations, labeled differently, could be detected simultaneously (Fig. 5) (67). Hotspot imaging is analogous to the approaches of other imaging techniques that employ radionuclides, such as positron emission tomography or single-photon emission tomography, albeit without the associated hazards of ionizing radiation. Although hotspot ^{19}F MRI images the labeled cells, anatomical ^{1}H MRI performed with the same scanner during the same MRI examination is superimposed without any image registration problems to precisely determine the biodistribution of the labeled cells. In this respect, MRI has clear advantages over conventional optical and nuclear imaging techniques.

PFCE has been used recently in different mixtures of lipids to formulate emulsified cationic and anionic nanoparticles, with and without the lipophilic gadolinium derivative Gd-DTPA-BOA, and including fluorescent rhodamine to tag different cells (66). Cationic nanoparticles showed, in all cases, a greater and more rapid uptake than anionic PFCE preparations (Fig. 6) (66). Different amounts of PFCE-labeled cells were injected into each hemisphere of a mouse brain, and then imaged with ^{19}F and ^{1}H MRI (Fig. 7). It was observed that the injected PFCE-labeled cells remained viable and were still rhodamine-positive, with no appreciable reduction in the fluorine signal, at least up to 2 weeks post-injection (66).

A different research area within molecular and cellular MRI is the use of transfected enzymes (reporter genes) that can convert a pro- (precursor) drug. In this technique, a gene with specific enzymatic activity is first introduced into tumor or other cells of interest. Then, a pro-drug is administered and, on internalization of the pro-drug into cells, it is converted by the transgene into an active drug. This method ensures that the drug will be active only in the target cells and will not affect other tissues. A similar example involves 5-FU, wherein yeast cytosine deaminase is introduced into an HT29 colon carcinoma cell line (83) to convert the precursor 5-fluorocytosine (5-FC) into 5-FU, and elicit a chemotherapeutic response. The formation of 5-FU, measured in xenografted tumors using ^{19}F MRS, provides an indication of the efficacy of drug delivery. By this means, ^{19}F MRS might provide a means of monitoring and optimizing the administration of such pro-drugs to patients for chemotherapy.

With regard to the use of ^{19}F probes as 'smart tracers' or 'molecular beacons', ^{19}F MRS has been employed to probe the enzymatic activity of a prototype reporter enzyme, β-galactosidase. This enzyme has been shown to liberate a glycone from the substrate 4-fluoro-2-nitrophenyl-β-D-galactopyranoside, resulting in a pH-dependent ^{19}F chemical shift of 5–10 ppm that can be used to measure intracellular pH (84). Other enzymes can be probed as well. For example, certain proteases (caspase-3), which are overexpressed in tumors, are able to cleave paramagnetic chelates from fluorinated molecules, thereby modulating ^{19}F relaxation times and signal intensity (85). Finally, temperature-sensitive liposomes containing ^{19}F tracers have been developed as beacons for image-guided drug delivery (86).

In addition to enzymes, fluorinated metabolic substrates are also potential targets of study that are accessible to ^{19}F MRI or MRS, when present in sufficient concentration. For example, the distribution of 2-fluoro-[^{18}F]-2-deoxy-glucose, a widely used positron emission tomography probe for the measurement of abnormal glucose consumption in tumors and ischemia, has been monitored with ^{19}F MRS after replacing the unstable ^{18}F atom with ^{19}F (87).

INCORPORATION OF PFCs INTO CELLULAR THERAPEUTIC BIOMATERIALS

The incorporation of PFCs into biomaterials is attractive for a number of reasons. By exploiting the various features of PFCs, fluorinated biomaterials can be used to create smart scaffolds that are capable of producing an oxygen-rich environment whilst permitting the noninvasive assessment of biological parameters, such as O_2 tension, pH and metabolite concentrations, with ^{19}F MRI. Fluorinated biomaterials, in conjunction with ^{19}F MRI, could thus provide important information on the delivery and long-term survival of cellular therapeutics. For these reasons, fluorinated biomaterials show promise for both the assessment and enhancement of the long-term viability of cellular therapeutics after transplantation.

To date, the use of fluorinated biomaterials has been limited to PFC-containing microcapsules. The use of microcapsules to provide the immuno-isolation of cellular therapeutics has clinical potential for a wide range of diseases that require enzyme or endocrine replacement therapy. A number of groups have explored the use of PFC-containing microcapsules. Barnett *et al*. (88) incorporated PFPE emulsions in alginate/poly-L-lysine (PLL) microcapsules to enable the assessment of the biodistribution and integrity of microcapsules with MRI. As PFCs are rapidly cleared from the body when they are no longer encapsulated, MRI could provide a means of assessing capsule rupture and loss of immunoprotection.

Other groups have used PFC-containing microcapsules for the determination of the local oxygen saturation *in vivo*. The paramagnetic properties of a polar oxygen affect the T_1 and chemical shift of ^{19}F nuclei in proportion to pO_2, as noted earlier, potentially enabling the use of microcapsular PFCs for the serial assessment of pO_2 *in vivo*. The first study of this type, by Nöth *et al*. (89), utilized PFC-loaded alginate capsules in conjunction with quantitative ^{19}F MRI to determine pO_2 inside capsules implanted in the peritoneal cavity and elsewhere in a rat (Fig. 8). Fraker *et al*. (90) later reported a related method using PFTA.

In addition to providing a means of assessing pO_2, PFCs can also increase local oxygen tension. The ability to increase oxygen availability provides added value for encapsulation therapy, where many studies have suggested that graft failure occurs because of the lack of vascular access for the encapsulated cells. This results in the gradual necrosis of implanted

cells. For this reason, the work of Khattak *et al*. (91) is particularly relevant. They found that the incorporation of a PFC emulsion in alginate micro-capsules increased significantly the viability of an immortalized hepatocyte cell line. They attributed this enhanced viability to the ability of the PFC reservoir to 'reload' itself with O_2 from plasma perfusing through the matrix – analagous to the O_2 transfer in emulsified PFCs that are currently being used for surgical applications (25). By acting as oxygen sinks, PFC-containing micro-capsules may have broad applications for increasing the viability of many encapsulated cell types.

In addition to increasing local oxygen concentrations, PFCs may enhance the immuno-isolation properties of alginate micro-capsules by modulating the immune response. *In vitro* studies have suggested that PFOB reduces cytokine release by human alveolar macrophages and attenuates oxidative injury in rat pulmonary artery endothelial cells. Furthermore, neutrophil adhesion to lung epithelial cells and subsequent cytolysis are inhibited by PFOB during activation with a pro-inflammatory stimulus (92), and PFOB attenuates neutrophil adhesion to activated endothelial cells (93). For these reasons, PFC-loaded alginate capsules could attenuate the rejection of cellular therapeutics in immunocompetent hosts.

As the incorporation of PFCs is not limited to alginate micro-capsules, further exploration of fluorinated biomaterials may prove to be attractive in tissue engineering. The unique behavior of PFCs, including their hydrophobic and lipophobic character and extreme inertness, nevertheless presents some significant design obstacles for direct incorporation into polymers. For this reason, only emulsified PFCs have been incorporated into biomaterials so far. Nevertheless, the many potential advantages of directly fluorinated biomaterials warrant future research in this area.

PHARMACOKINETICS AND TOXICITY OF PFCs

PFCs are chemically inert and stable compounds that are not metabolized and are excreted by normal clearance mechanisms, such as phagocytosis by the reticuloendothelial system, with eventual elimination by exhalation and bowel excretion (94). Most fluorocarbons within the molecular weight range of 460–520 Da are biologically inactive, and exhibit no significant toxicological risks, carcinogenicity or mutagenicity (23,25,95,96). The inertness of most of these compounds is an attractive property in many applications. However, environmental monitoring suggests that some degradation of PFCs into other persistent fluorinated chemicals can occur, and may demand recovery procedures, particularly for applications such as partial liquid ventilation (97).

PFCs for medical applications must be consistently prepared with high purity on a cost-effective basis that is typically large scale (25). Ideally, they should be excreted rapidly, which depends on their lipid solubility – the higher the better. This property is important for PFCs intended for intravascular use. Fluorocarbons containing other chemical elements, such as a terminal bromine atom, tend to be excreted more rapidly than predicted solely on the basis of their molecular weight (14). PFOB has been the subject of much of the research into PFC emulsions to date. Another factor to consider is the ease with which stable emulsions can be formed and sustained, as preparations must be able to withstand heat sterilization when required by regulatory agencies, such as the FDA (25), although irradiation or sterile filtration may be suitable alternatives.

The toxicity of organofluorinated compounds follows the same general principles with regard to the toxicity of drugs: it depends on the mechanism of action of the drug and the molecules generated by its metabolism, if any. Although not providing evidence of nontoxicity, when PFTA, PFOB or PFCE is injected into an animal, there is no significant difference between the *in vivo* and *in vitro* ^{19}F spectra of these molecules, consistent with their being resistant to metabolism, at least in the short term. However, another feature that

is often attributed to organofluorine compounds is their activity on the P450 enzyme system, which is important, as it relates to the elimination of many other drugs (98). Organofluorinated compounds seem to be associated with greater liver damage and interfere with thyroid hormones, when compared with their corresponding nonfluorinated analogs.

Highly fluorinated (carbon) compounds are not miscible with either aqueous or organic solvents. The smaller molecules tend to be cleared rapidly from the circulation, with brief retention in the mononuclear phagocyte system, mainly in the liver, spleen and bone marrow. PFTPA forms stable emulsions, but has a long retention time. Emulsions have been prepared with PFDC, which is rapidly cleared from the body, to take advantage of both effects.

PFCE and PFOB have been emulsified with pure lecithin, forming stable emulsions with small particle sizes (0.1–0.2 μm in diameter). Lecithin-based (and pluronic-based) emulsions show moderate inhibition of endotoxin-induced cytokine production, although they also cause substantial cytotoxicity in phagocytic cells after 24 h of incubation. After intravenous administration, PFC particles are taken up by the reticuloendothelial system, and evaporate through the lung, an elimination process that does not involve the breakdown of its chemical structure. Reports from a phase I clinical safety trial in healthy volunteers receiving PFOB (Table 2) indicated that the PFC emulsion does not affect coagulation (99,100).

The degradation products of some widely used fluorine-containing household chemicals (wetting agents, lubricants, corrosion inhibitors, insecticides, cosmetics, fire retardants and surfactants), such as perfluoro-octanoic acid, are known to induce peroxisome proliferation in hepatocytes, as well as considerable changes in enzymatic activity (101). The C–F bond is essentially xenobiotic and has an extremely high stability, making it resistant to degradation, even in volatile forms such as Freon. Fluorocarbons can accumulate in human tissues when inhaled, ingested or given intravenously. The length of time they remain in the body depends on their molecular weight and vapor pressure (volatility): the more volatile they are, the shorter their half-life, which can range from minutes to years. Indeed, evidence exists that there is long-term retention of some PFCs by the reticuloendothelial system (102). The major predictors for the diffusion of small molecules across cellular membranes are lipophilicity and molecular weight. The incorporation of fluorine into a drug can increase its lipophilicity and enhance its absorption into biological membranes. The small covalent radius of fluorine can facilitate the docking of drugs with their receptors. When the molecular weight of the fluorinated version of one drug is not significantly altered, passive diffusion should be comparable with that of the nonfluorinated form.

One fluorinated drug, fluoxetine hydrochloride (Prozac®), is a widely prescribed antidepressant in the world today. Fluoxetine is a potent inhibitor of serotonin. The brain tends to accumulate these agents at levels that are an order of magnitude higher than serum levels because of their lipophilicity and pH trapping in acidic vesicles. Based on data from 22 patients treated with fluoxetine, the brain concentration of the drug continues to increase long after its clinical effects are manifest, leveling off some 6–8 months after therapy commences (103). The drug accumulated to about 20 times the plasma level in these patients, although the brain concentration was not correlated with the clinical response. The study showed that, even 3.5 weeks after the end of drug therapy, a significant ^{19}F fluoxetine signal could be observed in the brain, suggesting a very long washout time. In another study, a weak correlation of fluoxetine level with positive clinical response was found in patients with social phobia (104).

Fluoxetine metabolizes to the therapeutically active compound norfluoxetine in the brain. Because the ^{19}F chemical shift of norfluoxetine is very close to that of fluoxetine, the two

compounds are not resolved *in vivo*. *In vitro* ^{19}F NMR studies of the extracts of both human and rat brain confirm that the *in vivo* signal arises roughly equally from fluoxetine and norfluoxetine.

CONCLUSIONS

As a result of their unique physicochemical properties, there is increasing interest in the use of fluorinated compounds in ^{19}F MRI and MRS to serve as biomedical contrast agents, biomarkers for monitoring the local physiological environment and indicators of therapy delivery vehicles, ranging from chemotherapeutic agents to cells to nanoparticles, in both experimental animal models and human studies. Some of these applications are already being used in patients, whereas others are on the verge of introduction to the clinic. Most of the recent studies have been performed at higher magnetic fields (1.5 T and above), as the low SNR remains a challenge because of the intrinsically low ^{19}F concentrations *in vivo*. The recent development of targeted and improved nanoparticle formulations with high payloads offers new promises for ^{19}F MRS and MRI applications in molecular and cellular imaging.

Acknowledgments

We are grateful to Mary McAllister for editing the manuscript. The authors were supported by the National Institute of Health with grant numbers RO1 EB007829 (PAB), RO1 EB007825 (JWMB), RO1 DA026299 (JWMB), 2RO1 NS045062 (JWMB), Roadmap R21 EB005252 (JWMB), NMSS RG3630 (JWMB), MSCRF-07-06-29-01 (JWMB) and the Maryland Nanotechnology Research and Industry Fund (MCINN SAF2008-05412).

Abbreviations used

BAPTA	1,2-bis(o-amino-phenoxy)ethane-N,N,N′,N′-tetraacetic acid
BOA	bis-oleate acid
DTPA	diethylenetriaminepentaacetate
EPI	echo planar imaging
FBAPTA	5,5′-difluoro-1,2-bis(o-amino-phenoxy) ethane-N,N,N′,N′-tetraacetic acid
5-FC	5-fluorocytosine
FDA	Food and Drug Administration
5-FU	5-fluorouracil
PFC	perfluorocarbon
PFCE	perfluoro-crown ether
PFDC	perfluorodecalin
PFOB	perfluoro-octyl bromide
PFPE	perfluoropolyether
PFTA	perfluorotributylamine
PFTPA	perfluorotripropylamine
pO_2	partial pressure of O2
SNR	signal-to-noise ratio
SPIO	super-paramagnetic iron oxide

References

1. Holland GN, Bottomley PA, Hinshaw WS. ^{19}F magnetic resonance imaging. J Magn Reson 1977;28:133–136.
2. Bulte JWM. Hot spot MRI emerges from the background. Nat Biotech 2005;23:945–946.
3. Clark LC, Gollan F. Survival of mammals breathing organic liquids equilibrated with oxygen at atmospheric pressure. Science 1966;152:1755–1756. [PubMed: 5938414]
4. Clark LC, Ackerman JL, Thomas SR, Millard RW, Hoffman RE, Pratt RG, Ragle-Cole H, Kinsey RA, Janakiraman R. Perfluorinated organic liquids and emulsions as biocompatible NMR imaging agents for ^{19}F and dissolved oxygen. Adv Exp Med Biol 1984;180:835–845. [PubMed: 6534151]
5. Thomas, SR. The biomedical application of fluorine-19 NMR. In: Partain, CI.; Patton, JA.; Kulkarni, MV.; James, AEJ., editors. Magnetic Resonance Imaging. Vol. 2. Saunders Co; London: 1988. p. 1536-1552.
6. Selinsky, BS.; Burt, CT. In vivo ^{19}F NMR. In: Berliner, LJ., editor. Biological Magnetic Resonance. Plenum Press; New York: 1992. p. 241-276.
7. London, RE. In vivo NMR studies utilizing fluorinated probes. In: Gillies, RJ., editor. Physiology and Biomedicine. Vol. 16. Academic Press; New York: 1994. p. 263-277.
8. Mason RP. Transmembrane pH gradients in vivo: measurements using fluorinated vitamin B6 derivatives. Curr Med Chem 1999;6:481–499. [PubMed: 10213795]
9. Bachert P. Pharmacokinetics using fluorine NMR in vivo. Progr NMR Spectr 1998;33:1–56.
10. Deutsch CJ, Taylor JS. Intracellular pH as measured by ^{19}F NMR. Ann NY Acad Sci 1987;508:33–47. [PubMed: 3501935]
11. Wolf W, Presant CA, Waluch V. ^{19}F-MRS studies of fluorinated drugs in humans. Adv Drug Deliv Rev 2000;41:55–74. [PubMed: 10699305]
12. McSheehy, PMJ.; Lemaire, LP.; Griffiths, JR. Fluorine-19 MRS: application in oncology. In: Grant, DM.; Harris, RK., editors. Encyclopedia of Nuclear Magnetic Resonance. Vol. 2. Wiley; New York: 1996. p. 2048-2052.
13. Zhao DW, Jiang L, Mason RP. Measuring changes in tumor oxygenation. Methods Enzymol 2004;386:378–418. [PubMed: 15120262]
14. Riess JG. Understanding the fundamentals of perfluorocarbons and perfluorocarbon emulsions relevant to in vivo oxygen delivery. Artif Cells Blood Substit Immobil Biotechnol 2005;33:47–63. [PubMed: 15768565]
15. Wolber J, Rowland IJ, Leach MO, Bifone A. Perfluorocarbon emulsions as intravenous delivery media for hyperpolarized xenon. Magn Reson Med 1999;41:442–449. [PubMed: 10204864]
16. Wolf W, Albright MJ, Silver MS, Weber H, Reichardt U, Sauer R. Fluorine-19 NMR spectroscopic studies of the metabolism of 5-fluorouracil in the liver of patients undergoing chemotherapy. Magn Reson Imaging 1987;5:165–169. [PubMed: 3626785]
17. Yu JX, Kodibagkar VD, Cui W, Mason RP. ^{19}F: a versatile reporter for non-invasive physiology and pharmacology using magnetic resonance. Curr Med Chem 2005;12:819–848. [PubMed: 15853714]
18. Brown JJ, Duncan JR, Heiken JP, Balfe DM, Corr AP, Mirowitz SA, Eilenberg SS, Lee JKT. Perfluoroctylbromide as a gastrointestinal contrast agent for MR imaging: use with and without glucagon. Radiology 1991;181:455–460. [PubMed: 1924788]
19. Anderson CM, Brown JJ, Balfe DM, Heiken JP, Borrello JA, Clouse RE, Pilgram TK. MR imaging of Crohn disease: use of perflubron as a gastrointestinal contrast agent. J Magn Reson Imaging 1994;4:491–496. [PubMed: 8061454]
20. Flacke S, Fischer S, Scott MJ, Fuhrhop RW, Allen JS, McLean M, Winter PM, Sicard GA, Gaffney PJ, Wickline SA, Lanza GM. Novel, MRI contrast agent for molecular imaging of fibrin: implications for detecting vulnerable plaques. Circulation 2001;104:1280–1285. [PubMed: 11551880]
21. Morawski AM, Winter PM, Crowder KC, Caruthers SD, Fuhrhop RW, Scott MJ, Robertson JD, Abendschein DR, Lanza GM, Wickline SA. Targeted nanoparticles for quantitative imaging of sparse molecular epitopes with MRI. Magn Reson Med 2004;51:480–485. [PubMed: 15004788]

22. Ahrens ET, Flores R, Xu H, Morel PA. In vivo imaging platform for tracking immunotherapeutic cells. Nat Biotech 2005;23:983–987.
23. Caruthers SD, Neubauer AM, Hockett FD, Lamerichs R, Winter PM, Scott MJ, Gaffney PJ, Wickline SA, Lanza GM. In vitro demonstration using ^{19}F magnetic resonance to augment molecular imaging with paramagnetic perfluorocarbon nanoparticles at 1.5 Tesla. Invest Radiol 2006;41:305–312. [PubMed: 16481914]
24. Janjic JM, Srinivas M, Kadayakkara DK, Ahrens ET. Self-delivering nanoemulsions for dual fluorine-19 MRI and fluorescence detection. J Am Chem Soc 2008;130:2832–2841. [PubMed: 18266363]
25. Krafft MP. Fluorocarbons and fluorinated amphiphiles in drug delivery and biomedical research. Adv Drug Deliv Rev 2001;47:209–228. [PubMed: 11311993]
26. Rafikova O, Sokolova E, Rafikov R, Nudler E. Control of plasma nitric oxide bioactivity by perfluorocarbons: physiological mechanisms and clinical implications. Circulation 2004;110:3573–3580. [PubMed: 15557364]
27. Krems B, Bachert P, Zabel WJ, Lorenz WJ. ^{19}F-[^{1}H] nuclear Overhauser effect and proton decoupling of 5-fluorouracil and alpha-fluoro-beta-alanine. J Magn Reson B 1995;108:155–164. [PubMed: 7648013]
28. Heidelberger C, Chaudhuri NK, Danneberg P, Mooren D, Griesbach L, Duschinsky R, Schnitzer RJ, Pleven E, Scheiner J. Fluorinated pyrimidines. A new class of tumor inhibitory compounds. Nature 1957;179:663–666. [PubMed: 13418758]
29. Shani J, Wolf W. A model of chemotherapy response to 5-FU in sensitive versus resistant lymphocytic leukemia in mice. Cancer Res 1977;37:2306–2308. [PubMed: 861951]
30. Stevens AN, Morris PG, Les RA, Sheldon PW, Griffiths JR. 5-Fluorouracil metabolism monitored in vivo by ^{19}F NMR. Br J Cancer 1984;50:113–117. [PubMed: 6743508]
31. O'Connell MJ, Martenson JA, Wieand HS, Krook JE, Macdonald JS, Haller DG, Mayer RJ, Gunderson LL, Rich TA. Improving adjuvant therapy for rectal cancer by combining protracted-infusion fluorouracil with radiation therapy after curative surgery. N Engl J Med 1994;331:502–507. [PubMed: 8041415]
32. Herskovic A, Martz K, Al-Sarraf M, Leichman L, Brindle J, Vaitkevicius V, Cooper J, Byhardt R, Davis L, Emami B. Combined chemotherapy and radiotherapy compared with radiotherapy alone in patients with cancer of the esophagus. N Engl J Med 1992;326:1593–1598. [PubMed: 1584260]
33. Fu KK. Radiation therapy with 5-fluorouracil in head and neck cancer. Semin Radiat Oncol 1997;7:274–282. [PubMed: 10717225]
34. Party UACTW. Epidermoid anal cancer: results from the UKCCCR randomised trial of radiotherapy alone versus radiotherapy, 5-fluorouracil, and mitomycin. Lancet 1996;348:1049–1054. [PubMed: 8874455]
35. Chakravarthy A, Abrams RA. Radiation therapy and 5-fluorouracil in pancreatic cancer. Semin Radiat Oncol 1997;7:291–299. [PubMed: 10717227]
36. Presant CA, Wolf W, Waluch V, Wiseman C, Kennedy P, Blayney D, Brechner RR. Association of intratumoral pharmacokinetics of fluorouracil with clinical response. Lancet 1994;343:1184–1187. [PubMed: 7909867]
37. Wolf W, Waluch V, Presant CA. Non-invasive 19F-MRS of 5-fluorouracil in pharmacokinetics and pharmacodynamic studies. NMR Biomed 1998;11:380–387. [PubMed: 9859944]
38. Martino R, Gilard V, Desmoulin F, Malet-Martino M. Fluorine-19 or phosphorus-31 NMR spectroscopy: a suitable analytical technique for quantitative in vitro metabolic studies of fluorinated or phosphorylated drugs. J Pharm Biomed Analysis 2005;38:871–891.
39. Deutsch, CJ.; Taylor, JS. ^{19}F NMR measurements of intracellular pH. In: Gupta, RK., editor. NMR Spectroscopy of Cells and Organisms. Vol. II. CRC Press, Inc; Boca Ratón, FL: 1987. p. 55-74.
40. Deutsch CJ, Taylor JS. New class of ^{19}F pH indicators: fluoroanilines. Biophys. J 1989;55:799–804.
41. Ojugo ASE, McSheehy PMJ, McIntyre DJO, McCoy C, Stubbs M, Leach MO, Judson IR, Griffiths JR. Measurement of the extracellular pH of solid tumours in mice by magnetic resonance

spectroscopy: a comparison of exogenous ^{19}F and ^{31}P probes. NMR Biomed 1999;12:495–504. [PubMed: 10668042]

42. Prior, MJW.; Maxwell, RJ.; Griffiths, JR. Fluorine ^{19}F NMR spectroscopy and imaging in vivo. In: Diehl, P.; Günther, H.; Kosfeld, R.; Seelig, J., editors. In Vivo Magnetic Resonance Spectroscopy III: In Vivo MR Spectroscopy: Potential and Limitations. Vol. 28. Springer-Verlag; Berlin: 1992. p. 101-130.
43. Mehta VM, Kulkarni PV, Mason RM, Constantinescu A, Aravind S, Goomer N, Antich PP. 6-Fluoropyridoxol a novel probe of cellular pH using ^{19}F NMR spectroscopy. FEBS Lett 1994;349:234–238. [PubMed: 8050572]
44. Gupta, RK.; Gillies, RJ. ^{19}F NMR measurement of intracellular free calcium ions in intact cells and tissues. In: Gupta, RK., editor. NMR Spectroscopy of Cells and Organisms. Vol. II. CRC Press, Inc; Boca Ratón, FL: 1987. p. 45-53.
45. Tsien RY. A non-disruptive technique for loading calcium buffers and indicators into cells. Nature 1981;290:527–528. [PubMed: 7219539]
46. Metcalfe JC, Hesketh TR, Smith GA. Free cytosolic Ca^{2+} measurements with fluorine labelled indicators using ^{19}F NMR. Cell Calcium 1985;6:183–195. [PubMed: 3874697]
47. Rinck PA. NMR-imaging von fluorhaltigen substanzen. Fortschr Rontgenstr 1984;140:239–243.
48. Perez-Sanchez JM, Pérez de Alejo R, Rodriguez I, Cortijo M, Peces-Barba G, Ruiz-Cabello J. In vivo diffusion weighted ^{19}F MRI using SF_6. Magn Reson Med 2005;54:460–463. [PubMed: 16032667]
49. Kuethe DO, Caprihan A, Gach M, Lowe IJ, Fukushima E. Imaging obstructed ventilation with NMR using inert fluorinated gases. J Appl Physiol 2000;88:2279–2286. [PubMed: 10846046]
50. Wolf U, Scholz A, Heussel CP, Markstaller K, Schreiber WG. Subsecond fluorine-19 MRI of the lung. Magn Reson Med 2006;55:948–951. [PubMed: 16534836]
51. Adolphi NL, Kuethe DO. Quantitative mapping of ventilation–perfusion ratios in lungs by ^{19}F MR imaging of T1 of inert fluorinated gases. Magn Reson Med 2008;59:739–746. [PubMed: 18383306]
52. Scholz AW, Wolf U, Fabel M, Weiler N, Heussel CP, Eberle B, David M, Schreiber WG. Comparison of magnetic resonance imaging of inhaled SF_6 with respiratory gas analysis. Magn Reson Imaging 2009;27:549–556. [PubMed: 18930366]
53. Schreiber WG, Eberle B, Laukemper-Ostendorf S, Markstaller K, Weiler N, Scholz A, Burger K, Heussel CP, Thelen M, Kauczor HU. Dynamic ^{19}F-MRI of pulmonary ventilation using sulfur hexafluoride (SF_6) gas. Magn Reson Med 2001;45:605–613. [PubMed: 11283988]
54. Ruiz-Cabello J, Perez-Sanchez JM, Perez deAlejo R, Rodríguez I, Gonzelez-Mangado N, Peces-Barba G, Cortijo M. Diffusion-weighted ^{19}F-MRI of lung periphery: influence of pressure and air–SF_6 composition on apparent diffusion coefficients. Respir Physiol Neurobiol 2005;148:43–46. [PubMed: 16098469]
55. Jacob RE, Chang YV, Choong CK, Bierhals A, Hu DZ, Zheng J, Yablonskiy DA, Woods JC, Gierada DS, Conradi MA. ^{19}F MR imaging of ventilation and diffusion in excised lungs. Magn Reson Med 2005;54:577–585. [PubMed: 16086368]
56. Conradi MS, Saam MS, Yablonskiy DA, Woods JC. Hyperpolarized ^{3}He and perfluorocarbon gas diffusion MRI of lungs. Progr NMR Spectr 2006;48:63–83.
57. Habib FA, Cohn SM. Blood substitutes. Curr Opin Anaesthesiol 2004;17:139–143. [PubMed: 17021542]
58. Spahn DR. Blood substitutes. Artificial oxygen carriers: perfluorocarbon emulsions. Crit Care 1999;3:R93–R97. [PubMed: 11094488]
59. Huang MQ, Ye Q, Williams DS, Ho C. MRI of lungs using partial liquid ventilation with water-in-perfluorocarbon emulsions. Magn Reson Med 2002;48:487–492. [PubMed: 12210913]
60. Laukemper-Ostendorf S, Scholz A, Burger K, Heussel CP, Schmittner M, Weiler N, Markstaller K, Eberle B, Kauczor H, Quintel M, Thelen M, Schreiber WG. ^{19}F-MRI of perflubron for measurement of oxygen partial pressure in porcine lungs during partial liquid ventilation. Magn Reson Med 2002;47:82–89. [PubMed: 11754446]
61. Wolfson MR. Novel applications and perfluorochemical-associated drug delivery. ASAIO J 2006;52:490.

62. Wauer RR, Gama de Abreu M, Rudiger M. 4th European Symposium on Perfluorocarbon Application. Eur J Med Res 2006;11 (Suppl 1):1–12. [PubMed: 17052973]
63. Constantino ML, Shaffer T, Wauer RR, Rüdiger M. The 5th European Symposium of Perfluorocarbon (PFC) Application. ASAIO J 2006;52:483. [PubMed: 16883132]
64. Kandler M, der Hardt KV, Chada M, Walther J, Schoof E, Dötsch J, Rascher W. 3rd European Symposium on Perfluorocarbon Application: Aerosolization of perfluorocarbons (aerosol-PFC): options and restrictions of pulmonary administration of aersolized perfluorocarbons. Eur J Med Res 2003;8:168–182.
65. Schlemmer HP, Becker M, Bachert P, Dietz A, Rudat V, Vanselow B, Wollensack P, Zuna I, Knopp MV, Weidauer H, Wannenmacher M, van Kaick G. Alterations of intratumoral pharmacokinetics of 5-fluorouracil in head and neck carcinoma during simultaneous radiochemotherapy. Cancer Res 1999;59:2363–2369. [PubMed: 10344745]
66. Ruiz-Cabello J, Walczak P, Kedziorek DA, Chacko VP, Schmieder AH, Wickline SA, Lanza GM, Bulte JW. In vivo 'hot spot' MR imaging of neural stem cells using fluorinated nanoparticles. Magn Reson Med 2008;60:1506–1511. [PubMed: 19025893]
67. Partlow KC, Chen J, Brant JA, Neubauer AM, Meyerrose TE, Creer MH, Nolta JA, Caruthers SD, Lanza GM, Wickline SA. ^{19}F magnetic resonance imaging for stem/progenitor cell tracking with multiple unique perfluorocarbon nanobeacons. FASEB J 2007;21:1647–1654. [PubMed: 17284484]
68. Sotak CH, Hees PS, Huang H-N, Hung M-H, Young SW. A new perfluorocarbon for use in fluorine-19 magnetic resonance imaging and spectroscopy. Magn Reson Med 1993;29:188–195. [PubMed: 8429782]
69. Dardzinski BJ, Sotak CH. Rapid tissue oxygen tension mapping using ^{19}F inversion-recovery echo-planar imaging of perfluoro-15-crown-5-ether. Magn Reson Med 1994;32:88–97. [PubMed: 8084241]
70. Lee H, Price RR, Holburn GE, Partain CL, Adams MD, Cacheris WP. In vivo fluorine-19 MR imaging: relaxation enhancement with Gd-DTPA. J Magn Reson Imaging 1994;4:609–613. [PubMed: 7949689]
71. Srinivas M, Morel PA, Ernst LA, Laidlaw DH, Ahrens ET. Fluorine-19 MRI for visualization and quantification of cell migration in a diabetes model. Magn Reson Med 2007;58:725–734. [PubMed: 17899609]
72. Börnet P, Norris DG, Koch H, Dreher W, Reichelt H, Leibfritz D. Fast perfluorocarbon imaging using ^{19}F U-FLARE. Magn Reson Med 1993;29:226–234. [PubMed: 8429787]
73. Gong B, Gill M, Washburn DB, Davenport WC, Adams D, Kwock L. Parameter optimization and calibration of ^{19}F magnetic resonance imaging at 1.5 tesla. Magn Reson Imaging 1991;9:101–106. [PubMed: 2056847]
74. Ratner AV, Quay S, Muller HH, Simpson BB, Hurd R, Young SW. F-19 relaxation rate enhancement and frequency shift Gd-DTPA. Invest Radiol 1989;24:224–227. [PubMed: 2753638]
75. Bulte JW, Kraitchman DL. Iron oxide MR contrast agents for molecular and cellular imaging. NMR Biomed 2004;17:484–499. [PubMed: 15526347]
76. Stuber M, Gilson WD, Schar M, Kedziorek DA, Hofmann LV, Shah S, Vonken EJ, Bulte JW, Kraitchman DL. Positive contrast visualization of iron oxide-labeled stem cells using inversion-recovery with ON-resonant water suppression (IRON). Magn Reson Med 2007;58:1072–1077. [PubMed: 17969120]
77. Cunningham CH, Arai T, Yang PC, McConnell MV, Pauly JM, Conolly SM. Positive contrast magnetic resonance imaging of cells labeled with magnetic nanoparticles. Magn Reson Med 2005;53:999–1005. [PubMed: 15844142]
78. Zurkiya O, Hu X. Off-resonance saturation as a means of generating contrast with superparamagnetic nanoparticles. Magn Reson Med 2006;56:726–732. [PubMed: 16941618]
79. Janjic JM, Ahrens ET. Fluorine-containing nanoemulsions for MRI cell tracking. Wiley Interdiscip Rev Nanomed Nanobiotechnol 2009;1:492–501. [PubMed: 19920872]
80. Nöth U, Morrissey SP, Deichmann R, Jung S, Adolf H, Haase A, Lutz J. Perfluoro-15-crown-5-ether labeled macrophages in adoptive transfer experimental allergic encephalomyelitis. Artif Cells Blood Substit Immobil Biotechnol 1997;25:243–254. [PubMed: 9167839]

81. Flogel U, Ding Z, Hardung H, Jander S, Reichmann G, Jacoby C, Schubert R, Schrader J. In vivo monitoring of inflammation after cardiac and cerebral ischemia by fluorine magnetic resonance imaging. Circulation 2008;118:140–148. [PubMed: 18574049]
82. Srinivas M, Turner MS, Janjic JM, Morel PA, Laidlaw DH, Ahrens ET. In vivo cytometry of antigen-specific T cells using ^{19}F MRI. Magn Reson Med 2009;62:747–753. [PubMed: 19585593]
83. Stegman LD, Rehemtulla A, Beattie B, Kievit E, Lawrence TS, Blasberg RG, Tjuvajev JG, Ross BD. Noninvasive quantitation of cytosine deaminase transgene expression in human tumor xenografts with in vivo magnetic resonance spectroscopy. Proc Natl Acad Sci USA 1999;96:9821–9826. [PubMed: 10449778]
84. Cui W, Otten P, Li Y, Koeneman KS, Yu J, Mason RP. Novel NMR approach to assessing gene transfection: 4-fluoro-2-nitrophenyl-beta-D-galactopyranoside as a prototype reporter molecule for beta-galactosidase. Magn Reson Med 2004;51:616–620. [PubMed: 15004806]
85. Mizukami S, Takikawa R, Sugihara F, Shirakawa M, Kikuchi K. Dual-function probe to detect protease activity for fluorescence measurement and ^{19}F MRI. Angew Chem Int Ed Engl 2009;48:3641–3643. [PubMed: 19353604]
86. Langereis S, Keupp J, van Velthoven JL, de Roos IH, Burdinski D, Pikkemaat JA, Grull H. A temperature-sensitive liposomal ^{1}H CEST and ^{19}F contrast agent for MR image-guided drug delivery. J Am Chem Soc 2009;131:1380–1381. [PubMed: 19173663]
87. Southworth R, Parry CR, Parkes HG, Medina RA, Garlick PB. Tissue-specific differences in 2-fluoro-2-deoxyglucose metabolism beyond FDG-6-P: a ^{19}F NMR spectroscopy study in the rat. NMR Biomed 2003;16:494–502. [PubMed: 14696007]
88. Barnett BP, Gilad AA, Ruiz-Cabello J, McMahon MT, Kraitchman DL, van Zijl PCM, Arepally A, Bulte JWM. Hot spot imaging of micro-capsules: an initial assessment of detection with ^{19}F and magnetization transfer imaging. Proc Int Soc Magn Reson Med 2006;14:1831.
89. Nöth U, Gröhn P, Jork A, Zimmermann U, Haase A, Lutz J. ^{19}F-MRI in vivo determination of the partial oxygen pressure in perfluorocarbon-loaded alginate capsules implanted into the peritoneal cavity and different tissues. Magn Reson Med 1999;42:1039–1047. [PubMed: 10571925]
90. Fraker, C.; Invaeradi, L.; Mares-Guia, M.; Ricordi, C. Novel polymer formulations containing perfluorinated compounds for the engineering of cells and tissues for transplantation that improves cell metabolism and survival, and methods for making same. PCT/US2000/000106, Patent No. WO/2000/040252.
91. Khattak SF, Chin KS, Bhatia SR, Roberts SC. Enhancing oxygen tension and cellular function in alginate cell encapsulation devices through the use of perfluorocarbons. Biotechnol Bioeng 2006;96:156–166. [PubMed: 16917927]
92. Rotta A, Gunnarsson B, Fuhrman B, Wiryawan B, Hernan L, Steinhorn D. Perfluorooctyl bromide (perflubron) attenuates oxidative injury to biological and nonbiological systems. Pediatr Crit Care Med 2003;4:233–238. [PubMed: 12749658]
93. Varani J, Hirschl R, Dame M, Johnson K. Perfluorocarbon protects lung epithelial cells from neutrophil-mediated injury in an in vitro model of liquid ventilation therapy. Shock 1996;6:339–344. [PubMed: 8946649]
94. Riess JG. Overview of progress in the fluorocarbon approach to in vivo oxygen delivery. Biomat Art Cells Immob Biotech 1992;20:183–202.
95. Flaim SF. Pharmacokinetics and side effects of perfluorocarbon-based blood substitutes. Artif Cells Blood Substit Immobil Biotechnol 1994;22:1043–1054. [PubMed: 7849908]
96. Lowe KC. Engineering blood: synthetic substitutes from fluorinated compounds. Tissue Eng 2003;9:389–399. [PubMed: 12857407]
97. Dunster KR, Davies MW, Fraser JF. An advanced expiratory circuit for the recovery of perfluorocarbon liquid from non-saturated perfluorocarbon vapour during partial liquid ventilation: an experimental model. Biomed Eng Online 2006;5:7. [PubMed: 16457722]
98. Poppers PJ. Hepatic drug metabolism and anesthesia. Anaesthesist 1980;29:55–58. [PubMed: 6990824]
99. Leese PT, Noveck RJ, Shorr JS, Woods CM, Flaim KE, Keipert PE. Randomized safety studies of intravenous perflubron emulsion. I. Effects on coagulation function in healthy volunteers. Anesth Analg 2000:804–811. [PubMed: 11004030]

100. Noveck RJ, Shannon EJ, Leese PT, Shorr JS, Flaim KE, Keipert PE, Woods CM. Randomized safety studies of intravenous perflubron emulsion. II. Effects on immune function in healthy volunteers. Anesth Analg 2000;91:812–822. [PubMed: 11004031]

101. Gilliland FD, Mandel JS. Serum perfluorooctanoic acid and hepatic enzymes, lipoproteins, and cholesterol: a study of occupationally exposed men. Am J Ind Med 1996;29:560–568. [PubMed: 8732932]

102. Pfannkuch F, Schnoy N. Perfluorochemical-emulsion (fluorocarbon-43) as blood gas carrier – fate of the substance after intravenous injection in rat (author's transl). Anaesthesist 1979;28:511–516. [PubMed: 393124]

103. Karson CN, Newton JEO, Livingston R, Jolly JB, Cooper TB, Sprigg J, Komoroski RA. Human brain fluoxetine concentrations. J Neuropsychiatr Clin Neurosci 1993;5:322–329.

104. Miner CM, Davidson JRT, Potts NLS, Tupler LA, Charles HC, Krishnan RKR. Brain fluoxetine measurements using fluorine magnetic resonance spectroscopy in patients with social phobia. Biol Psychiatry 1995;38:696–698. [PubMed: 8555383]

105. Martino R, Malet-Martino M, Gilard V. Fluorine nuclear magnetic resonance, a privileged tool for metabolic studies of fluoropyrimidine drugs. Curr Drug Metab 2000;1:271–303. [PubMed: 11465049]

106. Lee DJ, Burt CT, Koch RL. Percutaneous absorption of flurbiprofen in the hairless rat measured in vivo using ^{19}F magnetic resonance spectroscopy. J Invest Dermatol 1992;99:431–434. [PubMed: 1402001]

107. van Laarhoven HWM, Klomp DWJ, Kamm YJL, Punt CJA, Heerschap A. In vivo monitoring of capecitabine metabolism in human liver by ^{19}fluorine magnetic resonance spectroscopy at 1.5 and 3 Tesla field strength. Cancer Res 2003;63:7609–7612. [PubMed: 14633676]

108. Karson CN, Newton JE, Mohanakrishnan P, Sprigg J, Komoroski RA. Fluoxetine and trifluoperazine in human brain: a ^{19}F-nuclear magnetic resonance spectroscopy study. Psychiatry Res 1992;45:95–104. [PubMed: 1362616]

109. Strauss WL, Layton ME, Hayes CE, Dager SR. ^{19}F magnetic resonance spectroscopy investigation in vivo of acute and steady-state brain fluvoxamine levels in obsessive–compulsive disorder. Am J Psychiatry 1997;154:516–522. [PubMed: 9090339]

110. Strauss WL, Unis AS, Cowan C, Dawson G, Dager SR. Fluorine magnetic resonance spectroscopy measurement of brain fluvoxamine and fluoxetine in pediatric patients treated for pervasive developmental disorders. Am J Psychiatry 2002;159:755–760. [PubMed: 11986128]

111. Keston M, Brocklehurst JC. Flurazepam and meprobamate: a clinical trial. Age Ageing 1974;3:54–58. [PubMed: 4597061]

112. Henry ME, Moore CM, Kaufman MJ, Michelson D, Schmidt ME, Stoddard E, Vuckevic AJ, Berreira PJ, Cohen BM, Renshaw PF. Brain kinetics of paroxetine and fluoxetine on the third day of placebo substitution: a fluorine MRS study. Am J Psychiatry 2000;157:1506–1508. [PubMed: 10964871]

113. Henry ME, Schmidt ME, Hennen J, Villafuerte RA, Butma ML, Tran P, Kerner LT, Cohen BM, Renshaw PF. A comparison of brain and serum pharmacokinetics of R-fluoxetine and racemic fluoxetine: a 19-F MRS study. Neuropsychopharmacology 2005;30:1576–1583. [PubMed: 15886723]

114. Solomon B, Binns D, Roselt P, Weibe LI, McArthur GA, Cullinane C, Hicks RJ. Modulation of intratumoral hypoxia by the epidermal growth factor receptor inhibitor gefitinib detected using small animal PET imaging. Mol Cancer Ther 2005;4:417–422.

115. Snyder, WS.; Cook, MJ.; Nasset, ES.; Karhausen, LR.; Howells, GP.; Tipton, TH. CRP Publication. Vol. I. Pergamon Press; Oxford: 1984. Report of the Task Group on Reference Man; p. 23see Table 280–284

116. Cohen JL, Cheirif J, Segar DS, Gillam LD, Gottdiener JS, Hausnerova E, Bruns DE. Improved left ventricular endocardial border delineation and opacification with OPTISON (FS069), a new echocardiographic contrast agent: results of a phase III multicenter trial. J Am Coll Cardiol 1998;32:746–752. [PubMed: 9741522]

117. Kitzman DW, Godman ME, Gillam LD, Cohen JL, Aurigemman GP, Gottdiener JS. Efficacy and safety of the novel ultrasound contrast agent perflutren (definity) in patients with suboptimal

baseline left ventricular echocardiographic images. Am J Cardiol 2000;86:669–674. [PubMed: 10980221]

118. Wyrwicz AM, Pszenny MH, Schofield JC, Tilman PC, Gordon RE, Martin PA. Noninvasive observations of fluorinated anesthetics in rabbit brain by fluorine-19 nuclear magnetic resonance. Science 1983;222:428–430. [PubMed: 6623084]
119. Xu Y, Tang P, Zhang W, Firestone L, Winter PM. Fluorine-19 nuclear magnetic resonance imaging and spectroscopy of sevoflurane uptake, distribution, and elimination in rat brain. Anesthesiology 1995;83:766–774. [PubMed: 7574056]
120. Menon, DK. Fluorine-19 MRS: general overview and anesthesia. In: Harris, RK., editor. Encyclopedia of Nuclear Magnetic Resonance. Wiley; Chichester: 1995. p. 2052-2063.
121. Komoroski RA, Newton JE, Cardwell D, Sprigg J, Pearce J, Karson CN. In vivo ^{19}F spin relaxation and localized spectroscopy of fluoxetine in human brain. Magn Reson Med 1994;31:204–211. [PubMed: 8133756]
122. Menon DK, Lockwood GG, Peden CJ, Cox IJ, Sargentoni J, Bell JD, Coutts GA, Whitwam JG. In vivo fluorine-19 magnetic resonance spectroscopy of cerebral halothane in postoperative patients: preliminary results. Magn Reson Med 1993;30:680–684. [PubMed: 8139449]
123. Litt L, Gonzalez-Mendez R, James TL, Sessler DI, Mills P, Chew W, Moseley M, Pereira B, Severinghaus JW, Hamilton WK. An in vivo study of halothane uptake and elimination in the rat brain with fluorine nuclear magnetic resonance spectroscopy. Anesthesiology 1987;67:161–168. [PubMed: 3605742]
124. Mills P, Sessler DI, Moseley M, Chew W, Pereira B, James TL, Litt L. An in vivo 19 Fluorine nuclear magnetic resonance study of isoflurane elimination from the rabbit brain. Anesthesiology 1987;67:169–173. [PubMed: 3605743]
125. Litt L, Lockart S, Cohen Y, Yasuda N, Kim F, Freire B, Laster M, Peterson N, Taheri S, Chang LH, Sessler DI, Moseley M, Eger EI, James TL. In vivo 19 Fluorine nuclear magnetic resonance brain studies of halothane, isoflurane, and desflurane: rapid elimination and no abundant saturable binding. Ann NY Acad Sci 1991;929:707–724. [PubMed: 2058918]
126. Litt L. Nuclear magnetic resonance advance: imaging fluorinated anesthetics in the brain. Anesthesiology 1995;83:651–653. [PubMed: 7574042]
127. Dubois BW, Cherian SF, Evers AS. Volatile anesthetics compete for common binding sites on bovine serum albumin: a ^{19}F NMR study. Proc Natl Acad Sci USA 1993;90:6478–6482. [PubMed: 8341659]
128. Cosgrove DO, Blomley MJK, Eckersley RJ, Harvey C. Innovative contrast specific imaging with ultrasound. Electromedica 70 2002;2:147–150.
129. Gould SA, Rosen AL, Sehgal LR, Sehgal HL, Langdale LA, Krause LM, Rice CL, Chamberlin WH, Moss GS. Fluosol-DA as a red-cell substitute in acute anemia. New Engl J Med 1986;314:1653–1656. [PubMed: 3713771]
130. Pisani E, Tsapis N, Paris J, Nicolas V, Cattel L, Fattal E. Polymeric nano/ microcapsules of liquid perfluorocarbons for ultrasonic imaging: physical characterization. Langmuir 2006;2006:4397–4402. [PubMed: 16618193]
131. Ceckler TL, Gibson SL, Hilf R, Bryant RG. In situ assessment of tumor vascularity using fluorine NMR imaging. Magn Reson Med 1990;13:416–433. [PubMed: 2325542]
132. Cuignet OY, Wood BL, Chandler WL, Spiess BD. A second-generation blood substitute (perfluorodichlorooctane emulsion) generates spurious elevations in platelet counts from automated hematology analyzers. Anesth Analg 2000;90:517–522. [PubMed: 10702429]
133. Briceno JC, Rincon IE, Velez JF, Castro I, Arcos MI, Velasquez CE. Oxygen transport and consumption during experimental cardiopulmonary bypass using oxyfluor. ASAIO J 1999;45:322–327. [PubMed: 10445739]
134. Mattrey RF. Perfluorooctylbromide: a new contrast agent for CT, sonography, and MR imaging. Am J Roentgenol 1989;152:247–252. [PubMed: 2643258]
135. Cyrus T, Abendschein DR, Caruthers SD, Harris TD, Glattauer V, Werkmeister JA, Ramshaw JAM, Wickline SA, Lanza GM. MR three-dimensional molecular imaging of intratumoral biomarkers with targeted nanoparticles. J Cardiovasc Magn Reson 2006;8:535–541. [PubMed: 16755843]

136. Mason RP, Rodbumrung W, Antich PP. Hexafluorobenzene: a sensitive [19]F NMR indicator of tumor oxygenation. NMR Biomed 1996;9:125–134. [PubMed: 8892399]

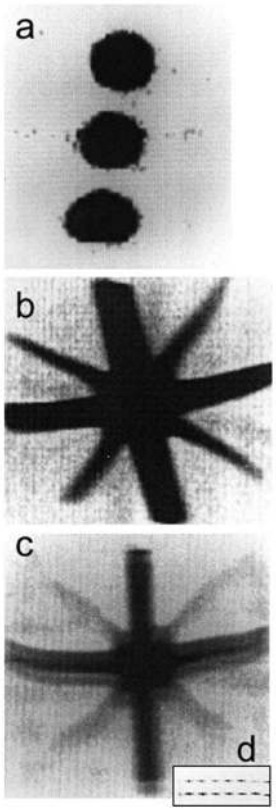

Figure 1.
The first ^{19}F images from 1977 (1). (a) ^{19}F MRI of three tubes of 1.4 M NaF with resolution of about 0.13 *T*0.13 *T*3 mm^3. (b, c) ^{19}F MRI of a perfluorocarbon (PFC), perfluorotributylamine, in a star-shaped 'Union Jack' phantom made from 2-mm (diagonal) and 6-mm tubes. The resolution is halved to about 0.6 *T*0.6 mm^2. All images were acquired in about 400 s at 0.7 T using a steady-state free-precession (SSFP) MRI sequence (TR of several milliseconds). In (c), the image bandwidth per point is reduced, resulting in signal-to-noise ratio (SNR) loss and a 'ghost' image or 'chemical shift artifact' from the two chemically shifted moieties of this PFC, which are about 6 ppm apart. The two peaks are seen directly when the gradient in the vertical direction is switched off in the inset (d). Adapted, with permission, from Holland *et al*. (1).

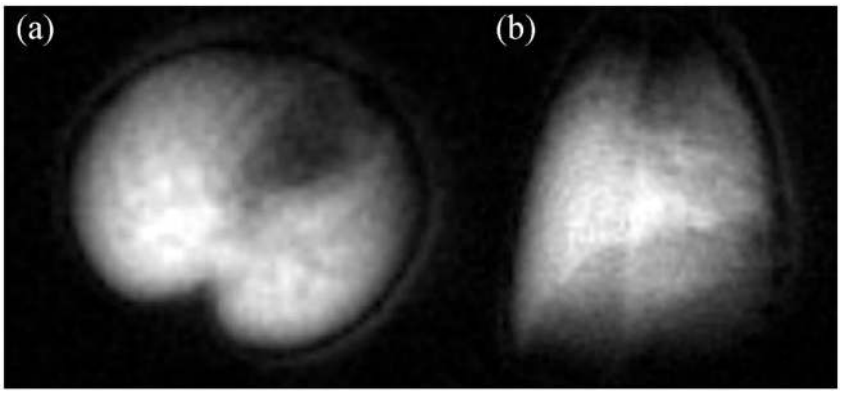

Figure 2.
Post-mortem ^{19}F MRI of lung gas density using C_2F_6. Axial images (a) were acquired within 2 min and coronal images (b) were acquired within 3 min using a 4.7-T magnet. These images show excellent quality similar to that obtained with hyperpolarized gases, although with much more accumulation.

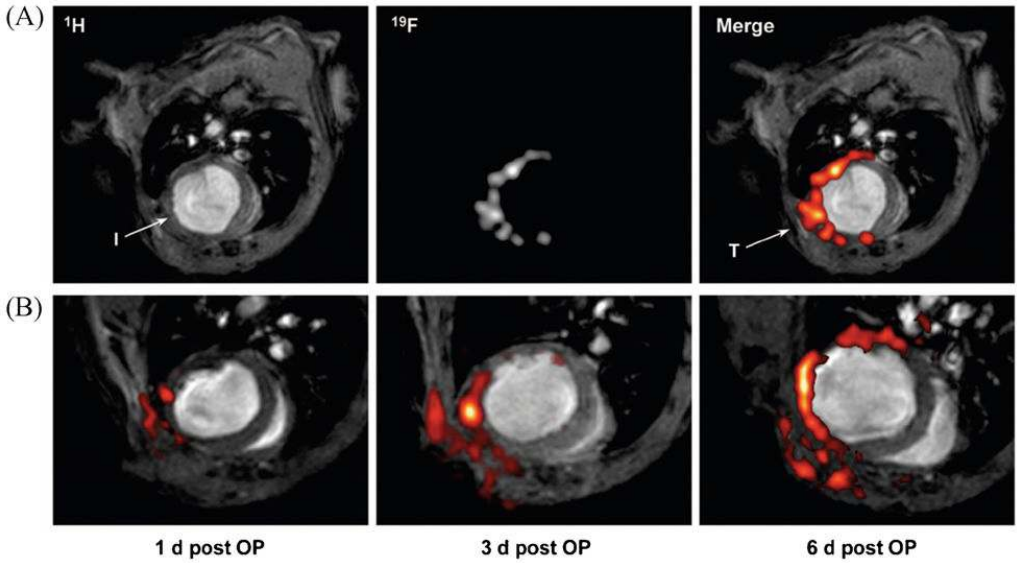

Figure 3.

Infiltration of perfluorocarbons (PFCs) after myocardial infarction as detected by *in vivo* ^{19}F MRI. (a) Anatomically corresponding ^{1}H and ^{19}F images from the mouse thorax recorded 4 days after ligation of the left anterior descending coronary artery, showing accumulation of ^{19}F signal near the infarcted region (I) and at the location of surgery where the thorax was opened (T). PFCs were injected at day 0 (2 h after infarction) via the tail vein. (b) Sections of ^{1}H images superimposed with the matching ^{19}F images (red) acquired 1, 3 and 6 days after surgery (post OP) indicate a time-dependent infiltration of PFCs into injured areas of the heart and the adjacent region of the chest affected by thoracotomy. At day 4, an additional bolus of PFCs was injected to compensate for clearance of the particles from the bloodstream after 3 days. Subsequent histology demonstrated that the uptake of PFCs had occurred in cells of the monocyte/macrophage lineage. Reproduced, with permission, from Flogel *et al*. (81).

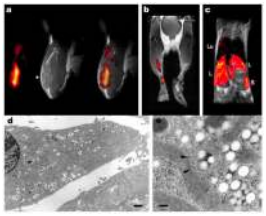

Figure 4.
In vivo ^{19}F MRI of perfluoro-crown ether (PFCE)-labeled dendritic cells in a mouse. (a) Mouse quadriceps after intramuscular injection of PFCE-labeled cells. From left to right are ^{19}F, ^{1}H and a composite ^{19}F/^{1}H image. (b) Composite image of dendritic cell migration into the popliteal lymph node following a hind foot pad injection. (c) Composite image through the torso following intravenous inoculation with perfluoropolyether (PFPE)-labeled cells. Cells are apparent in the liver (L), spleen (S) and, sporadically, lungs (Lu). Electron micrograph of a labeled fetal skin-derived dendritic cell line at a low magnification (d) and a higher magnification (e). Particles (100–200 nm) appear as smooth spheroids. Arrows show a typical multiple-membrane compartment enclosing these particles. Adapted, with permission, from Ahrens *et al*. (22).

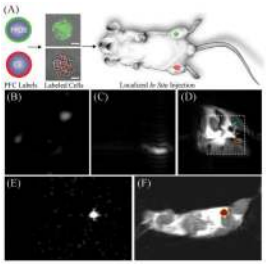

Figure 5.

Localization of labeled cells after *in situ* injection. (a) To determine the utility for cell tracking stem/progenitor cells labeled with either perfluoro-octyl bromide (PFOB) (green) or perfluoro-crown ether (PFCE) (red), nanoparticles were locally injected into mouse thigh skeletal muscle. (b–d) At 11.7 T, spectral discrimination permits the imaging of the fluorine signal attributable to ~ 1×10^6 PFOB-loaded (b) or PFCE-loaded (c) cells individually which, when overlaid onto a conventional ^{1}H image of the site (d), reveals PFOB- and PFCE-labeled cells localized to the left and right leg, respectively (broken line indicates 3×3-cm^2 field of view for ^{19}F images). (e, f) Similarly, at 1.5 T, ^{19}F image of ~ 4×10^6 PFCE-loaded cells (e) locates to the mouse thigh in a ^{1}H image of the mouse cross-section (f). The absence of background signal in ^{19}F images (b, c, e) enables unambiguous localization of PFCE-containing cells at both 11.7 and 1.5 T. Reproduced, with permission, from Partlow *et al*. (67). PFC, perfluorocarbon.

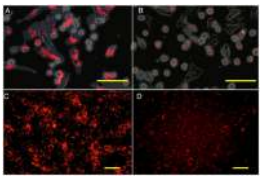

Figure 6.
Fluorescence microscopy of cationic (a, c) and anionic (b, d) perfluoro-crown ether (PFCE)-labeled C17.2 mouse neural stem cells after 4 h of incubation with 2.4 mM PFCE. (a, b) Rhodamine fluorescent (red) and phase contrast overlay image of cells immediately after 4 h of incubation. (c,d) Rhodamine fluorescent images of cells cultured for an additional 18 h after removal of PFCE at 4 h of incubation. Note the transport and intracellular redistribution of label between the two time points. Scale bars: 100 μm in (a, b) and 50 μm in (c, d). Reproduced, with permission, from Ruiz-Cabello *et al*. (66).

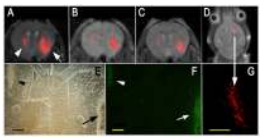

Figure 7.
In vivo MRI of transplanted C17.2 neural stem cells, with the ^{19}F signal superimposed on the ^{1}H MR images. (a–c) MR images at 1 h (a), 3 days (b) and 7 days after injection of 4×10^4 (left hemisphere, arrowhead in a) or 3×10^5 (right hemisphere, arrow in a) cationic perfluoro-crown ether (PFCE)-labeled cells. (e, f) Corresponding histopathology at day 7 with phase contrast (e) and anti-β-gal immunohistochemistry (f) demonstrates that implanted cells remain viable and continue to produce the marker enzyme. In (f), the right arrow indicates cells migrating from the injection site into the brain parenchyma. (d) MR image of a different animal at 14 days after injection of equal amounts of 4×10^5 C17.2 cells in both hemispheres, demonstrating the persistence of the ^{19}F signal for 2 weeks. (g) Corresponding histopathology showing rhodamine fluorescence from PFCE-labeled cells co-localizing with the ^{19}F signal. Scale bar, 500 μm. Reproduced, with permission, from Ruiz-Cabello *et al*. (66).

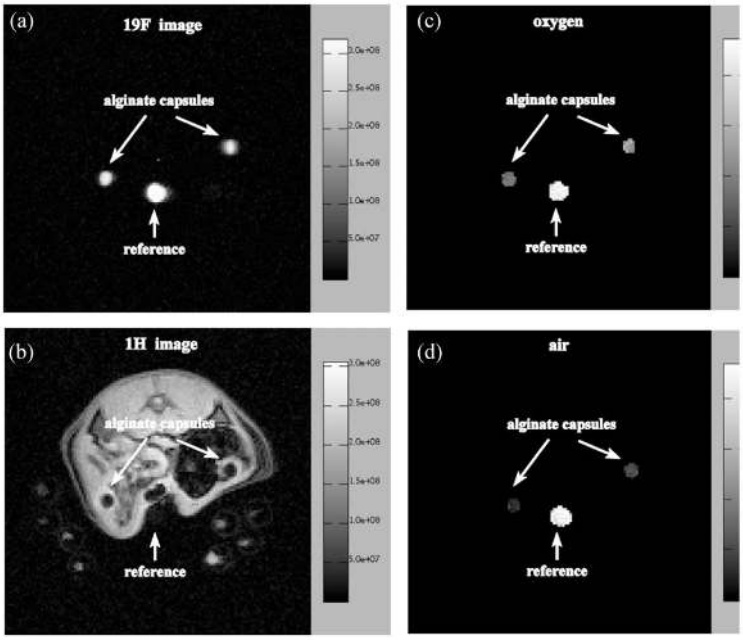

Figure 8.

^{19}F (a) and ^{1}H (b) images of a 2-mm transaxial slice through the peritoneal cavity of a rat showing two alginate capsules loaded with pure *trans*-1,2-bis(perfluorobutyl)-ethylene (F-44E), and the calculated ^{19}F pO_2 maps of the same slice whilst the animal is breathing oxygen (c) and air (d). The average pO_2 values in the alginate capsules are 9.0 ± 1.4% (left capsule) and 12.8 ± 2.0% (right capsule) in (c) and 3.2 ± 1.0% (left capsule) and 5.0 ± 1.4% (right capsule) in (d). Images were acquired on day 1 after implantation. The scale on the right of (a) and (b) gives the signal intensity in arbitrary units; the scale in (c) and (d) gives the pO_2 values in per cent. 100% corresponds to 760 mmHg. Reproduced, with permission, from Nöth *et al*. (89).

Table 1

List of ^{19}F drugs and therapeutic agents

Agent	Commercial name or acronym	Chemical formula	Modality	Application	Physical state	Relative SNR[a] (reference)
5,5′-Difluoro-1,2-bis (*o*-amino-phenoxy) ethane-*N*,*N*,*N*′,*N*′-tetraacetic acid	FBAPTA	$C_{22}H_{22}F_2N_2O_{10}$	MRS	Calcium chelator	Solution	2.1×10^{-5} (46)
5-Fluorouracil	Efudex®	$C_4H_3FN_2O_2$	MRI, MRS	Antineoplastic	Saline solution	1.0×10^{-5} (8,12,27,30,34,36–38,42,105)
Flurbiprofen	Adfeed, Ansaid	$C_{15}H_{13}FO_2$	MRS	Anti-inflammatory	Gel, oral tablets	1.0×10^{-5} (106)
Fluorodeoxyglucose	FDG	$C_6H_{11}FO_5$	MRS	Inhibitor	Solution	1.0×10^{-5} (17) [b]
Deoxyfluouridine (pro-drug)	Capecitabine (Xeloda®)	$C_{15}H_{22}FN_3O_6$	MRS	Prodrugs, antineoplastic	Oral tablets, injectable	1.0×10^{-5} (105,107)
Fluoxetine hydrochloride	Prozac®	$C_{17}H_{18}F_3NO$, HCl	MRS	Antidepressant	Capsule, liquid solutions	3.1×10^{-5} (108)
Fluvoxamine	Dumirox	$C_{15}H_{21}F_3N_2O_2$	MRS	Antidepressant	Oral tablet	3.1×10^{-5} (109,110)
Flurazepam	Dalmane, Felison	$C_{21}H_{23}ClFN_3O$	MRS	Anti-anxiolytic	Capsule	1.0×10^{-5} (111)
Fluoexetine	Prozac®, Sarafem®	$C_{17}H_{18}F_3NO$	MRS	Antidepressant	Capsule, syrup	3.1×10^{-5} (112,113)
Floxuridine	Fudr®	$C_9H_{11}FN_2O_5$	MRS	Antineoplastic	Injectable	1.0×10^{-5} (107)
Gefinitib	Iressa®	$C_{22}H_{24}ClFN_4O_3$	MRS	Antineoplastic	Oral tablet	1.0×10^{-5} (114)

[a] ^{19}F signal-to-noise ratio (SNR) of the fluorinated agent at a concentration of 1 μmol/g wet tissue weight relative to the ^{1}H signal detected from an equivalent tissue volume with a detector coil of the same geometry. The calculation assumes a tissue water content of 76.5% (± 0.37 SD), which is an average of the water contents of brain, skeletal muscle and liver tissues (115), and sample-dominant noise resulting in a linear-dependent SNR with field strength.

[b] And references therein.

Table 2

List of volatile ^{19}F agents

Agent	Commercial name or acronym	Chemical formula	Modality	Application	Physical state	Relative SNR[a]	Reference
Linear perfluorocarbons (e.g. tetrafluoromethane, hexafluoroethane, fluoropropane, etc.)	Optison™, Perflutren	CF_4, C_2F_6, C_3F_8, etc.	MRI, US	Respiratory and cardiac imaging	Gas dispersion (lipid microsphere) in a injectable suspension	(4, 6, 8, etc.) $\times 10^{-5}$	(116,117)
Anesthetics (e.g. halothane, isoflurane, sevoflurane, desflurane, methoxyflurane)	Forane®, Ultane®, Suprane®, Analgizer, Inhalan	$C_2HBrClF_3$ (halothane)	MRI, MRS	General anesthesia	Volatile liquids for inhalation administered via vaporizer	3.1×10^{-5}	(118–127)
		$C_3H_2ClF_5O$ (isofluorane)				5.2×10^{-5}	
		$C_4H_3F_7O$ (sevofluorane)				7.3×10^{-5}	
		$C_3H_2F_6O$ (desflurane)				6.3×10^{-5}	
		$C_3H_4Cl_2F_2O$ (methoxyflurane)				2.1×10^{-5}	
Sulfur hexafluoride	SonoVue®	SF_6	MRI, US	Vent, cardiac and microvasculature imaging	Gas: SonoVue® is a gas dispersion in a liquid (NaCl)	6.3×10^{-5}	(128)

US, ultrasound.

[a] ^{19}F signal-to-noise ratio (SNR) of the fluorinated agent at a concentration of 1 μmol/g wet tissue weight relative to the ^{1}H signal detected from an equivalent tissue volume with a detector coil of the same geometry. The calculation assumes a tissue water content of 76.5% (± 0.37 SD), which is an average of the water contents of brain, skeletal muscle and liver tissues (115), and sample-dominant noise resulting in a linear-dependent SNR with field strength.

Table 3

List of liquid ^{19}F agents

Agent	Commercial name or acronym	Chemical formula	Modality	Application	Physical state in normal conditions	Relative SNR[a]	Reference
Perfluorotripropylamine, perfluorodecalin	Fluosol-DA®, PFTPA	$C_9F_{21}N$	MRI	BS, OS	Liquid emulsion (20%), Fluosol® discontinued	2.2×10^{-4}	(4,129)
Perfluorodecalin	Perflunafene, PFDC	$C_{10}F_{18}$	MRI	BS, OS	Liquid emulsion (20%), longer blood half-life	1.9×10^{-4}	(4,130)
Perfluorotributylamine	Oxypherol™, PFTA	$C_{12}F_{27}N$	MRI	BS, OS	Liquid emulsion	2.8×10^{-4}	(131)
Perfluorodichlorooctane	PFDCO, Oxyfluor	$C_8F_{16}C_{12}$	MRI, US	BS, OS, CL	Liquid emulsion (40%)	1.7×10^{-4}	(132,133)
Perfluorooctylbromide, perflubron	LiquiVent®, Oxygent™, PFOB, Imagent™, Oxycyte™	$C_8F_{17}Br$	MRI, MRS, CT	BS, OS, CL, GI	Liquid emulsion (60%) Oral administration in some cases	1.8×10^{-4}	(18,130,134,135)
		$C_8F_{16}O_4$				1.7×10^{-4}	
		$(CF_2CF_2O)_4$				1.7×10^{-4}	
		$C_{10}F_{20}O_5$				2.1×10^{-4}	
	12-crown-4-ether, 15-crown-5-ether, 18-crown-6-ether	$(CF_2CF_2O)_5$				2.1×10^{-4}	
		$C_{12}F_{24}O_6$				2.5×10^{-4}	
Perfluoro-poly-ethers		$(CF_2CF_2O)_6$	MRI, MRS	OS, CL	Liquid emulsions (20–40%)	2.5×10^{-4}	(22,67,69)
Fluorinated aromatics, e.g. hexafluorobenzene		C_6F_6	MRI, MRS	OS	Liquid	6.3×10^{-5}	(136)

BS, blood substitute; OS, oxygen sensor; CL cell labeling; CT, computed tomography; GI, gastrointestinal; US, ultrasound.

[a] ^{19}F signal-to-noise ratio (SNR) of the fluorinated agent at a concentration of 1 μmol/g wet tissue weight relative to the ^{1}H signal detected from an equivalent tissue volume with a detector coil of the same geometry. The calculation assumes a tissue water content of 76.5% (± 0.37 SD), which is an average of the water contents of brain, skeletal muscle and liver tissues (115), and sample-dominant noise resulting in a linear-dependent SNR with field strength.